Article

Depolarization of Cardiac Membrane Potential Synchronizes Calcium Sparks and Waves in Tissue

Daisuke Sato,[1,*] Daniel C. Bartos,[1] Kenneth S. Ginsburg,[1] and Donald M. Bers[1,*]
[1]Department of Pharmacology, University of California, Davis, Davis, California

ABSTRACT The diastolic membrane potential (V_m) can be hyperpolarized or depolarized by various factors such as hyperkalemia or hypokalemia in the long term, or by delayed afterdepolarizations in the short term. In this study, we investigate how V_m affects Ca sparks and waves. We use a physiologically detailed mathematical model to investigate individual factors that affect Ca spark generation and wave propagation. We focus on the voltage range of −90 ~ −70 mV, which is just below the V_m for sodium channel activation. We find that V_m depolarization promotes Ca wave propagation and hyperpolarization prevents it. This finding is directly validated in voltage clamp experiments with Ca waves using isolated rat ventricular myocytes. Ca transport by the sodium-calcium exchanger (NCX) is determined by V_m as well as Na and Ca concentrations. Depolarized V_m reduces NCX-mediated efflux, elevating $[Ca]_i$, and thus promoting Ca wave propagation. Moreover, depolarized V_m promotes spontaneous Ca releases that can cause initiation of multiple Ca waves. This indicates that during delayed afterdepolarizations, Ca release units (CRUs) interact with not just the immediately adjacent CRUs via Ca diffusion, but also further CRUs via fast (~0.1 ms) changes in V_m mediated by the voltage and Ca-sensitive NCX. This may contribute significantly to synchronization of Ca waves among multiple cells in tissue.

INTRODUCTION

Premature ventricular contractions (PVC) are thought to trigger cardiac arrhythmias (1–3). One cause of PVCs is delayed afterdepolarizations (DAD), due to transient inward currents (4–7). The transient inward current, carried mostly via the sodium-calcium exchanger (NCX), becomes larger, especially when spontaneous calcium (Ca) releases from the sarcoplasmic reticulum (SR) initiate Ca waves (8). However, Ca waves in a single cell will not cause PVCs in tissue because cells are coupled by gap junctions and surrounding cells keep the membrane potential (V_m) too negative for sodium (Na) channel activation. This is often called source-sink mismatch (9,10). To overcome the source-sink mismatch and initiate PVCs, Ca waves must occur simultaneously in multiple cells (9,11). However, because diffusion of Ca between cells is slow, especially when $[Ca]_i$ is elevated (12,13), most Ca waves cannot propagate across the cell membrane to adjacent cells. In this study, we show that Ca waves can be synchronized in multiple cells during DADs via voltage and Ca-sensitive NCX.

MATERIALS AND METHODS

Mathematical model

We used a physiologically detailed mathematical model of a ventricular myocyte to investigate individual factors that affect Ca spark initiation and wave propagation. Our base model is a subcellular Ca cycling model recently developed by Restrepo et al. (14). In this model, there are 19,305 (65 × 27 × 11) Ca release units (CRUs), which are coupled by Ca diffusion through cytosol and network SR. Each CRU contains 100 ryanodine receptors (RyRs). The RyR is described by a four-state Markovian model and each RyR opens stochastically depending on cleft space Ca concentration ($[Ca]_{Cleft}$) and junctional SR Ca concentration ($[Ca]_{SR}$). The detailed formulation of the model is in the Supporting Material and our previous work (15).

We focused on the voltage range of −90 ~ −70 mV. We chose relatively high intracellular Na concentrations ($[Na]_i$), 12–14 mM, to mimic the $[Na]_i$ reached just after the fast pacing where DADs often occur (16) and the $[Na]_i$ that was measured in paced rabbit ventricular myocytes from failing hearts (17). In this study, we blocked Na current to avoid initiation of action potentials and the L-type Ca current to avoid initiation of Ca waves by L-type Ca channel openings, although the open probability and its V_m sensitivity are relatively small near the resting V_m.

Isolation of rat cardiac myocytes

Ventricular myocytes from Sprague Dawley rats were isolated as previously described (18). Rats were anesthetized using 3% isoflurane. Hearts were rapidly excised and perfused on a Langendorff apparatus for 5 min with minimal essential medium (MEM) at 37°C gassed with 100% O_2 before addition of 0.05 mg/mL Liberase TH (Roche-Life Science). Triturates were incubated for 10 min at 37°C in the same enzyme solution. Cells were then settled by gravity, washed 2–3× with 0 mM Ca^{2+} MEM with 2% bovine serum albumin (to stop enzymatic reactions), and kept in 0 mM Ca^{2+} MEM until use. All animal procedures were approved by the University of California, Davis Institutional Animal Care and Use Committee in accordance with the National Institutes of Health (NIH) Guide for the Care and Use of Laboratory Animals.

Laser scanning confocal Ca^{2+} imaging and electrophysiology

Cells were plated on laminin-coated glass coverslips in 0 mM Ca^{2+} normal Tyrode's (NT) solution containing (in mM) 140 NaCl, 4 KCl, 1 $MgCl_2$, 10

Submitted November 4, 2013, and accepted for publication July 15, 2014.
*Correspondence: dsato@ucdavis.edu or dmbers@ucdavis.edu
Editor: Godfrey Smith.

0006-3495/14/09/1313/5 $2.00
http://dx.doi.org/10.1016/j.bpj.2014.07.053

glucose, and 5 HEPES (pH 7.4 with NaOH). Intact myocytes were loaded with 5 μM Fluo-4 AM (Molecular Probes-Life Technologies) for 28 min, and then washed 3× with 0 mM Ca^{2+} NT. The dyes were allowed to further deesterify for 20 min in 0 Ca^{2+} NT. Whole-cell patch clamp, using pipettes with resistances ranging from 2 to 3 MΩ, was used to control V_m. The internal pipette solution contained (in mM) 90 aspartic acid (K^+ salt), 40 KCl, 10 NaCl, 5.5 $MgCl_2$, 5 ATP, 10 HEPES, and 0.05 Fluo-4 K^+ (Molecular Probes-Life Technologies) (pH 7.2 with KOH). An Axopatch-200B patch clamp amplifier and pCLAMP10.4 software (Axon Instruments) were used. Only cells with membrane resistances >1 GΩ were used for analyses. Once intracellular access was obtained, bath [Ca] ($[Ca^{2+}]_e$) was increased to 3 mM to promote Ca^{2+} wave propagation. From a holding potential of −100 mV, V_m was depolarized to −70 mV for up to 5–8 min and then repolarized to −100 mV. At each potential Ca^{2+} was imaged using a Biorad Radiance 2100 laser scanning confocal microscope equipped with a Nikon Plan Fluor 40× oil lens. Fluo-4 was excited at 488 nM and emission was recorded using a 500/530 nM bandpass filter at 166 lines/s. Image analysis was done with ImageJ. All experiments were performed at room temperature (21–25°C).

Statistics

Data were reported as the mean ± SE. A one-way ANOVA with Tukey post hoc analysis was performed to determine if values were different from control. A *P*-value below 0.05 was considered statistically significant.

RESULTS AND DISCUSSION

The life of the Ca wave has three steps: initiation, propagation, and termination. Increased numbers and further propagation of Ca waves contribute to both the amplitude of DADs and a propensity toward PVCs. First, we investigate how V_m affects Ca wave propagation in a single cell. Isolated Ca sparks become Ca waves as SR Ca load becomes higher. In our model, this occurs around $[Ca]_{SR}$ ~ 1300 μM when $[Na]_i$ = 14 mM (Fig. S1 in the Supporting Material). Note that these numbers would be affected by various factors such as RyR/calsequestrin mutations and up(down)regulation of SERCA. We measure the probability of successful wave propagation, defining success as propagation from one end of the cell to the other end in the longitudinal direction. We initiate the Ca wave by stimulating CRUs within the five leftmost sarcomeres. V_m plays its most critical role when the cell condition is close to the transition from Ca sparks to Ca waves. At $[Ca]_{SR}$ = 1300 μM, most Ca waves cannot propagate successfully at V_m more negative than −85 mV (Fig. 1 *A*). However, once V_m reaches ~−70 mV, 38% of Ca waves propagate successfully (*green curve* in Fig. 1 *A*). If $[Ca]_{SR}$ is elevated to 1400 μM, >95% of Ca waves propagate when V_m = −70 mV. However, at V_m more negative than −85 mV, more than half of the Ca waves fail to propagate (*red curve* in Fig. 1 *A*). The strength and direction of NCX operation are also a function of $[Na]_i$. Even 2 mM higher $[Na]_i$ reduces Ca efflux and thus elevates $[Ca]_i$, further promoting successful Ca wave propagation at a given SR load and V_m (*solid lines* versus *dashed lines* in Fig. 1 *A*).

Ca waves may terminate before they reach the other end of the cell. This phenomenon has been observed experimentally as miniwaves. The incidence of miniwaves under the conditions in Fig. 1 *A* is 1 — the indicated probability. Even under conditions largely favoring miniwaves, depolarization of V_m also lengthens them and promotes transient inward currents (Fig. 1 *B*).

A Ca wave is initiated by spontaneous Ca sparks. Therefore, as spontaneous Ca releases occur more frequently, Ca waves can be initiated more frequently. In our previous study (19), we showed that NCX suppresses spontaneous Ca sparks by reducing Ca-induced Ca release in the cleft space. Here, we show that changing diastolic V_m also strongly affects Ca spark-mediated SR Ca release. At relatively modest SR Ca loading, $[Ca]_{SR}$ = 700 μM, as V_m depolarizes from −90 to −70 mV, Ca spark-mediated SR Ca release increases by 36% for $[Na]_i$ = 14 mM (Fig. 2; shown as the summation of spark fluxes). This effect is larger for higher $[Na]_i$ (*solid* versus *dashed lines* in Fig. 2).

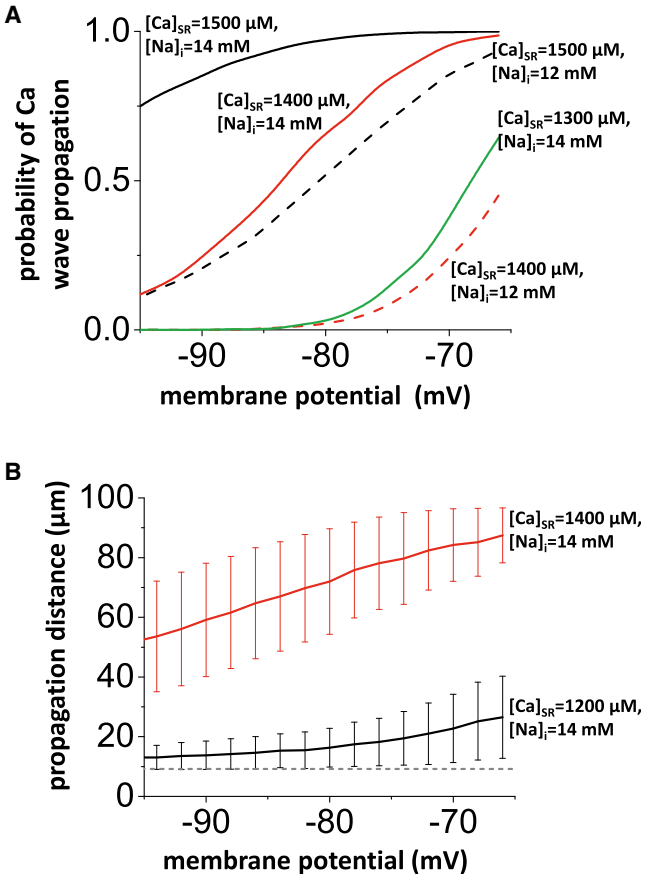

FIGURE 1 (*A*) The probability of successful wave propagation increases at more depolarized V_m. V_m was clamped and did not change during this simulation. The simulation was done in a 50 × 5 × 5 CRU cell. Solid lines and dashed lines are results for $[Na]_i$ = 14 and 12 mM, respectively. (*B*) The propagation distance of Ca waves versus the V_m. Solid lines are average and error bars are standard deviation. CRUs within the 5 leftmost sarcomeres were stimulated to initiate waves. Therefore, 9.2 μm (=5 × 1.84 μm, *dashed line*) should be subtracted for the actual propagation distance. The cell length was 92 μm; therefore, a distance of 46 μm was 50% of cell length, and so on. To see this figure in color, go online.

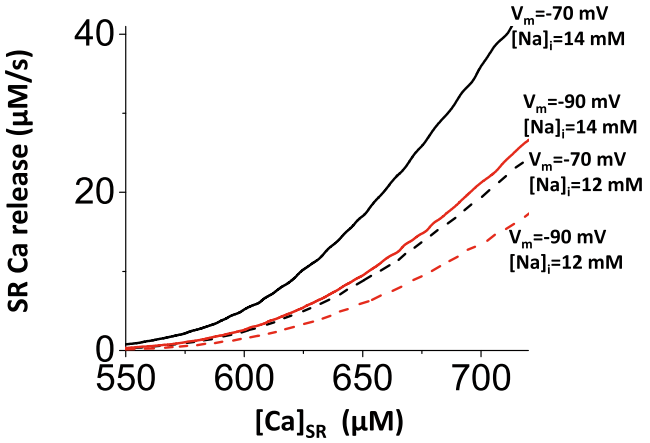

FIGURE 2 Ca spark-mediated SR Ca release (*steady-state leak*) vs. $[Ca]_{SR}$ at $V_m = -90$ and -70 mV. Solid lines (*dashed lines*) are results for $[Na]_i = 14$ (12) mM. To see this figure in color, go online.

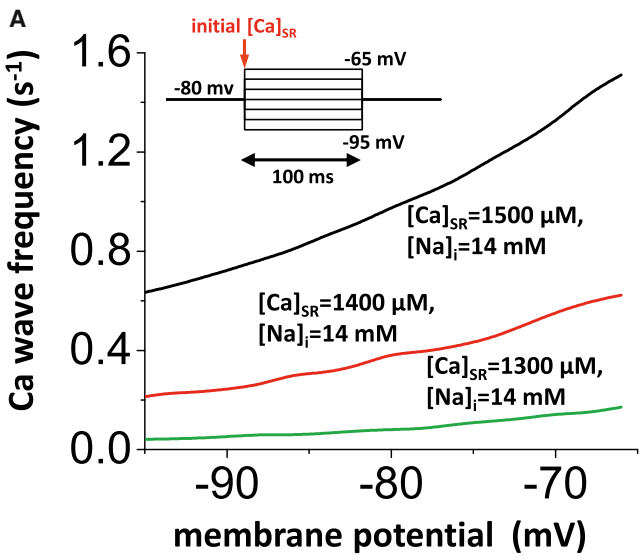

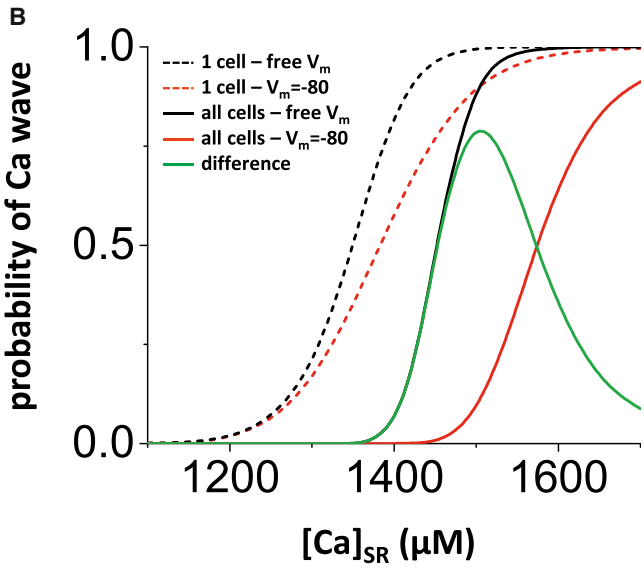

FIGURE 3 (*A*) Frequency of Ca waves versus holding V_m for initial $[Ca]_{SR} = 1300$, 1400, and 1500 μM. $[Na]_i$ was 14 mM. Ca waves were measured for 100 ms in each simulation. The frequency was calculated by the number of waves observed/(the number of trial $\times$ 0.1). (*B*) The probability of spontaneous Ca waves in tissue (5×5 cells). Ca waves were measured for 300 ms in each simulation. Dashed lines: probability in an individual cell. Solid lines: probability that spontaneous Ca waves occurred in all 25 cells. Black: free V_m (where V_m can be depolarized via transient inward currents). Red: V_m was held at -80 mV. Green: The difference between black and red traces shows the additional probability of waves attributable to V_m depolarization. Note that Na and Ca channels were blocked so that the excitation of the action potential could not synchronize Ca sparks and waves. To see this figure in color, go online.

As V_m is depolarized, more Ca waves propagate successfully as macro or full Ca waves (Fig. 1). The frequency of Ca sparks, which may initiate Ca waves, is also increased (Fig. 2). These results imply that the frequency of Ca waves will be increased during DADs. We applied a voltage clamp protocol (Fig. 3 *A*, *inset*) to mimic DADs and measured the frequency of Ca waves (Fig. 3 *A*). As V_m depolarized, incidence of Ca waves increased. For example, the frequency was doubled as V_m depolarized from -90 to -70 mV at $[Ca]_{SR} = 1500$ μM.

Finally, we tested the effect of V_m depolarization in tissue with V_m unclamped ($5 \times 5 = 25$ cells). Cells are coupled via gap junctions. Na and L-type Ca currents were blocked, so that depolarization is entirely due to the transient inward current caused by spontaneous Ca releases. The probability (p_{single}) of Ca wave occurrence in an individual cell is increased as $[Ca]_{SR}$ is increased (Fig. 3 *B*, *dashed black line*). The solid black line indicates the probability of a Ca wave in all 25 cells. Red curves are results when V_m of tissue is held at -80 mV (*dashed curve* for one cell, *solid curve* for 25 cells). In this case, electrotonic coupling has no influence and the result is identical to that in isolated myocytes. For this clamped case, the cells are independent, so that the probability that Ca waves occur synchronously in all 25 cells is $(p_{single})^{25}$ (*solid red line*). Even if V_m is held, Ca waves still can occur synchronously as $[Ca]_{SR}$ is increased and the mechanism of synchronization is essentially the mechanism proposed by Wasserstrom et al. (20); see below. Therefore the difference (Fig. 3 *B*, *green curve*) is the additional probability due to the synchronization effect of V_m depolarization. This is maximized when $[Ca]_{SR}$ is in the transition region between no Ca wave and spontaneous Ca waves ($[Ca]_{SR} = 1400 \sim 1500$ μM in Figs. 3 *B* and Fig. S1).

To validate our model for how diastolic changes of V_m affect the probability of Ca wave propagation in a native system, we performed whole-cell patch clamp and confocal Ca imaging simultaneously on freshly isolated rat ventricular myocytes. From a hyperpolarized V_m of -100 mV, myocytes were depolarized to -70 mV and then repolarized to -100 mV. At each potential, the probability of Ca wave propagation was determined (Fig. 4). We found a

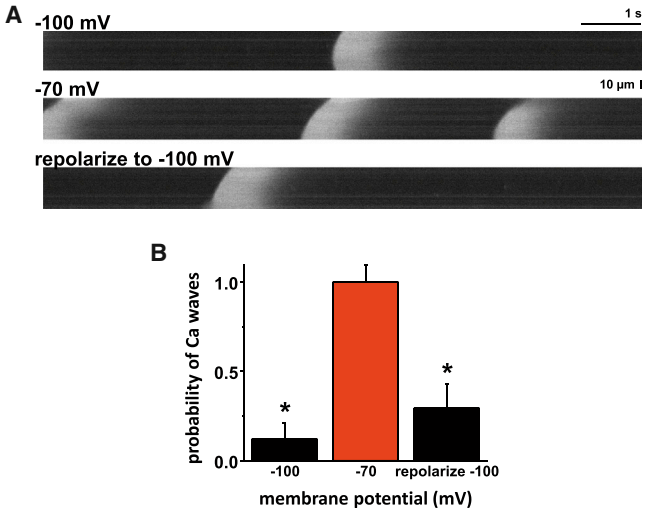

FIGURE 4 (*A*) Representative steady-state Ca waves in an individual voltage clamped myocyte. The cell was initially hyperpolarized at V_m −100 mV, depolarized to −70 mV, and finally repolarized to −100 mV. (*B*) Average probability of Ca wave formation in myocytes, each initially held at −100 mV, then depolarized to −70 mV, and finally repolarized to −100 mV. ($n = 7$ cells, $^*P < 0.05$) To see this figure in color, go online.

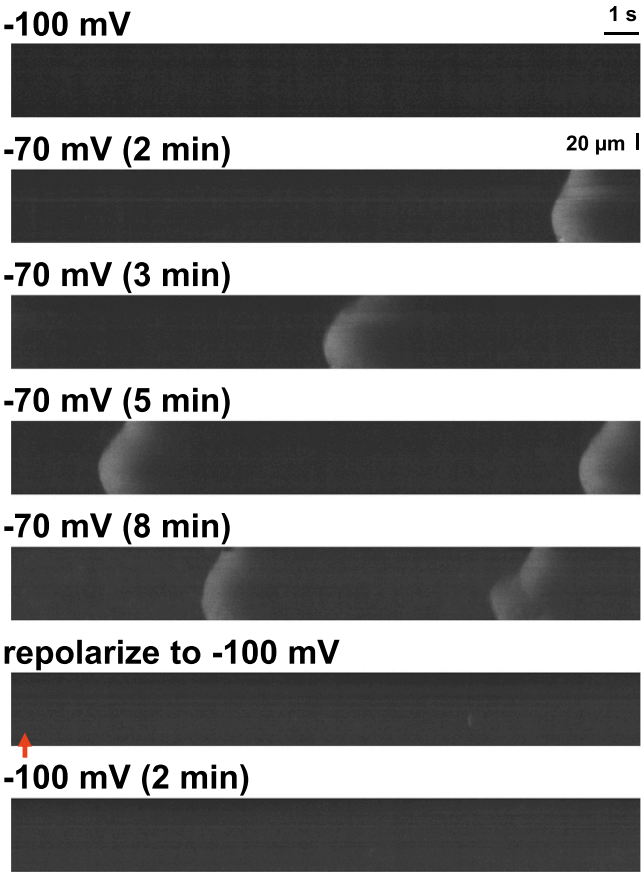

FIGURE 5 Representative example showing an individual myocyte where waves formed initially on depolarization from V_m −100 to −70 mV at a frequency that stabilized during 2–8 min. Waves terminated abruptly on repolarization to −100 mV. The red arrow indicates when the V_m was changed and the time after the V_m was changed is indicated in parentheses. To see this figure in color, go online.

significantly larger propensity for Ca wave occurrence when myocytes were depolarized, compared to both the initial condition and upon repolarization at −100 mV (Fig. 4 *A*: representative example from an individual myocyte; Fig. 4 *B*: probability based on $n = 7$ experiments). All cells initiated waves within 1–2 min when held depolarized at −70 mV, but only 3 out of 7 cells displayed any waves when held at −100 mV. This experiment is complicated by potential time-dependent changes in SR Ca content. That is, SR Ca content may be higher during the steady state at −70 mV vs. −100 mV.

In Fig. 5 we tested whether acute hyperpolarization to –100 mV could immediately halt periodic Ca waves seen at –70 mV (before progressive changes in SR Ca content). In this cell, there were no waves at −100 mV, but after the step to −70 mV there was a progressive development of Ca waves, which reached a steady state of ~2 waves per image (18 s) in 2–8 min at −70 mV. At the arrow, V_m was clamped to −100 mV and Ca waves disappeared immediately.

These data suggest that changes in V_m can rapidly influence the probability of spontaneous Ca waves. Of course further gradual increases in $[Ca]_{SR}$ in response to depolarization (again via NCX-dependent shifts in Ca) should lead to further increased Ca spark frequency and probability of Ca wave formation.

A Ca wave propagates when Ca sparks recruit new sparks in the adjacent CRUs. When SR Ca release events occur, the released Ca is removed mostly via the SERCA pump and the NCX from the cytosol. If this removal process dominates over the positive feedback process of Ca-induced Ca release, Ca waves cannot propagate. Diastolic V_m can be hyperpolarized or depolarized by various factors such as hypo- or hyperkalemia in the long term, or depolarized by DADs in the short term. Myocytes coupled to fibroblasts also have less negative resting V_m (21). In this study, we have investigated how hyperpolarized or depolarized V_m affect Ca wave initiation and propagation.

Our experimental and mathematical results show that depolarization of V_m promotes Ca wave propagation and hyperpolarization prevents Ca wave propagation. Near the resting V_m, electrogenic NCX works in the forward mode, namely, as one Ca ion leaves the cell, three Na ions enter the cell. In an unclamped cell, this current depolarizes the cell membrane. Ca transport by NCX is determined by V_m as well as [Na] and [Ca]. Depolarized V_m reduces NCX-mediated efflux, so that local $[Ca]_i$ does not decay, but rather can rise. Thus, depolarization promotes spontaneous Ca sparks and Ca wave propagation.

Recently, Wasserstrom et al. showed that Ca waves can be synchronized in multiple cells (20), which are driven by

common conditions. In their study, although Ca waves in different cells are functionally independent and do not interact directly, they occur synchronously when the probability of Ca waves increases, dictated mainly by a characteristic time required for SR Ca reloading and RyR recovery, i.e., SR Ca load and RyR in all cells are reset at each paced beat.

In this study, we show an additional mechanism of synchronization of Ca waves among multiple cells in tissue. CRUs interact with the immediately adjacent CRUs via both cytosolic and SR Ca diffusion. Ca diffusion between cells is not sufficient to synchronize waves (22) because of limited intercellular diffusion of Ca through gap junctions (12,13). However, when Ca sparks, and especially Ca waves occur, Ca efflux via NCX depolarizes V_m, which spreads in tissue quickly through gap junctions (effective diffusion coefficient $D_v = G_i/(S_v \cdot C_m) \sim 1.0\ cm^2/s$ (23), where G_i is the intercellular conductivity, S_v is the surface volume ratio of the cell, and C_m is the cell capacitance). In contrast, $D_{Ca} \sim 1.4 \sim 3.5 \times 10^{-6}\ cm^2/s$ (24) even within a cell and diffusion of Ca between cells is lower than this value). Thus, depolarization has more efficacy than Ca diffusion to promote Ca sparks and Ca wave propagation among multiple cells.

CONCLUSION

CRUs interact with not only just the adjacent CRUs via Ca diffusion, but also further CRUs via V_m, as mediated by voltage and Ca-sensitive NCX. Our finding provides a potentially strong causal mechanism for synchronization of Ca waves in tissue and sheds light on understanding of PVC formation.

SUPPORTING MATERIAL

One figure, mathematical model, and supporting references are available at http://www.biophysj.org/biophysj/supplemental/S0006-3495(14)00800-5.

This work was supported by National Institutes of Health grant K99-HL111334 (to D.S.) and National Institutes of Health grant R37-HL30077 and R01-HL105242 (to D.M.B.).

REFERENCES

1. Nuyens, D., M. Stengl, …, P. Carmeliet. 2001. Abrupt rate accelerations or premature beats cause life-threatening arrhythmias in mice with long-QT3 syndrome. *Nat. Med.* 7:1021–1027.
2. Engel, G., J. G. Beckerman, …, P. J. Wang. 2004. Electrocardiographic arrhythmia risk testing. *Curr. Probl. Cardiol.* 29:365–432.
3. Messineo, F. C. 1989. Ventricular ectopic activity: prevalence and risk. *Am. J. Cardiol.* 64:53J–56J.
4. Pogwizd, S. M., and D. M. Bers. 2002. Calcium cycling in heart failure: the arrhythmia connection. *J. Cardiovasc. Electrophysiol.* 13:88–91.
5. Janse, M. J. 1999. Electrophysiology of arrhythmias. *Arch. Mal. Coeur Vaiss.* 92:9–16.
6. Bers, D. M., S. Despa, and J. Bossuyt. 2006. Regulation of Ca2+ and Na+ in normal and failing cardiac myocytes. *Ann. N. Y. Acad. Sci.* 1080:165–177.
7. Schlotthauer, K., and D. M. Bers. 2000. Sarcoplasmic reticulum Ca(2+) release causes myocyte depolarization. Underlying mechanism and threshold for triggered action potentials. *Circ. Res.* 87:774–780.
8. Katra, R. P., and K. R. Laurita. 2005. Cellular mechanism of calcium-mediated triggered activity in the heart. *Circ. Res.* 96:535–542.
9. Xie, Y., D. Sato, …, J. N. Weiss. 2010. So little source, so much sink: requirements for after depolarizations to propagate in tissue. *Biophys. J.* 99:1408–1415.
10. Rohr, S., J. P. Kucera, …, A. G. Kléber. 1997. Paradoxical improvement of impulse conduction in cardiac tissue by partial cellular uncoupling. *Science.* 275:841–844.
11. Myles, R. C., L. Wang, …, C. M. Ripplinger. 2012. Local β-adrenergic stimulation overcomes source-sink mismatch to generate focal arrhythmia. *Circ. Res.* 110:1454–1464.
12. Spray, D. C., J. H. Stern, …, M. V. Bennett. 1982. Gap junctional conductance: comparison of sensitivities to H and Ca ions. *Proc. Natl. Acad. Sci. USA.* 79:441–445.
13. Noma, A., and N. Tsuboi. 1987. Dependence of junctional conductance on proton, calcium and magnesium ions in cardiac paired cells of guinea-pig. *J. Physiol.* 382:193–211.
14. Restrepo, J. G., J. N. Weiss, and A. Karma. 2008. Calsequestrin-mediated mechanism for cellular calcium transient alternans. *Biophys. J.* 95:3767–3789.
15. Sato, D., and D. M. Bers. 2011. How does stochastic ryanodine receptor-mediated Ca leak fail to initiate a Ca spark? *Biophys. J.* 101:2370–2379.
16. Faber, G. M., and Y. Rudy. 2000. Action potential and contractility changes in [Na(+)](i) overloaded cardiac myocytes: a simulation study. *Biophys. J.* 78:2392–2404.
17. Despa, S., M. A. Islam, …, D. M. Bers. 2002. Intracellular Na(+) concentration is elevated in heart failure but Na/K pump function is unchanged. *Circulation.* 105:2543–2548.
18. Li, Y., E. G. Kranias, …, D. M. Bers. 2002. Protein kinase A phosphorylation of the ryanodine receptor does not affect calcium sparks in mouse ventricular myocytes. *Circ. Res.* 90:309–316.
19. Sato, D., S. Despa, and D. M. Bers. 2012. Can the sodium-calcium exchanger initiate or suppress calcium sparks in cardiac myocytes? *Biophys. J.* 102:L31–L33.
20. Wasserstrom, J. A., Y. Shiferaw, …, G. L. Aistrup. 2010. Variability in timing of spontaneous calcium release in the intact rat heart is determined by the time course of sarcoplasmic reticulum calcium load. *Circ. Res.* 107:1117–1126.
21. Camelliti, P., T. K. Borg, and P. Kohl. 2005. Structural and functional characterisation of cardiac fibroblasts. *Cardiovasc. Res.* 65:40–51.
22. Aistrup, G. L., J. E. Kelly, …, J. A. Wasserstrom. 2006. Pacing-induced heterogeneities in intracellular Ca2+ signaling, cardiac alternans, and ventricular arrhythmias in intact rat heart. *Circ. Res.* 99:e65–e73.
23. Winfree, A. T. 1998. A spatial scale factor for electrophysiological models of myocardium. *Prog. Biophys. Mol. Biol.* 69:185–203.
24. Soeller, C., and M. B. Cannell. 1997. Numerical simulation of local calcium movements during L-type calcium channel gating in the cardiac diad. *Biophys. J.* 73:97–111.

Supplemental Materials

Depolarization of cardiac membrane potential synchronizes calcium sparks and waves in tissue

Daisuke Sato, Daniel C Bartos, Kenneth S Ginsburg, and Donald M Bers

$[Ca]_{SR}$ dependence

Ca waves are observed as $[Ca]_{SR}$ >1000 μM. Most Ca waves are mini waves when $[Ca]_{SR}$ is lower than 1500 μM, but as $[Ca]_{SR}$ increases toward ~1700 μM, most Ca waves become macro or full waves which propagate until the end of the cell walls.

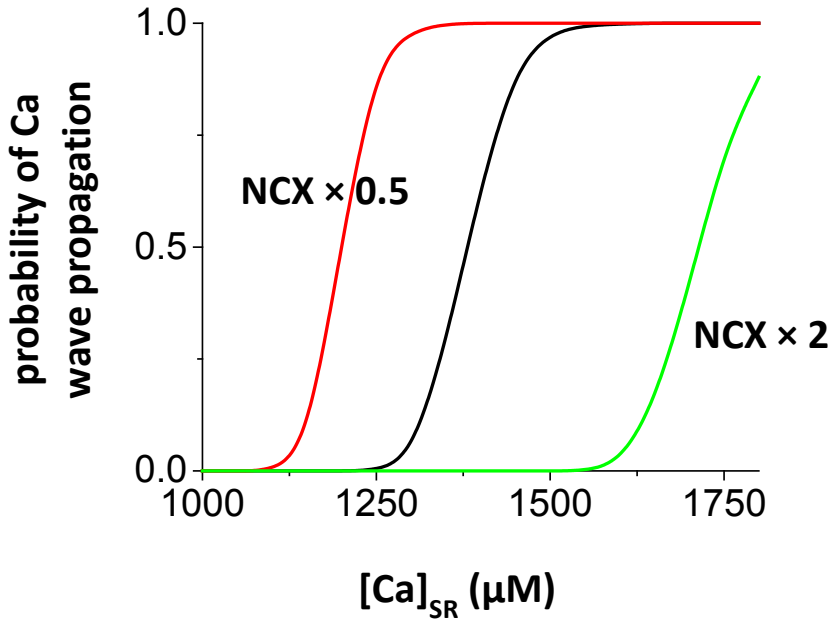

Figure S1 The probability of successful wave propagation vs $[Ca]_{SR}$. Ca waves occur more frequently as $[Ca]_{SR}$ is increased (black). The membrane potential was held at -80 mV. Therefore, NCX works in the forward mode. The position of the curve depends on the conductance or expression of NCX (red: NCX ×0.5; green: NCX × 2; black: normal NCX). $[Na]_i$=14 mM.

Mathematical model

We used a physiologically detailed mathematical model of a ventricular myocyte to investigate individual factors which affect Ca wave propagation. Our base model is a subcellular Ca cycling model recently developed by Restrepo et al (1). The dimension of this model is 121 μm × 25 μm × 11 μm and there are 19305 (65×27×11) Ca release units (CRUs) and each CRU contains one hundred RyR channels. The RyR model is a four-state Markovian model. Each RyR opens stochastically depending on $[Ca]_{Cleft}$ and $[Ca]_{SR}$. The separations of CRU are 1.84 μm and 0.9 μm in the longitudinal and transverse directions, respectively. The major difference from the previous versions of this model is Ca diffusion in submembrane space. There is diffusion in the transverse direction but not in the longitudinal direction, based on the fact that most T-tubules are aligned only transversely. We also added the background sarcolemmal membrane Ca flux (I_{CaBk}) and the sarcolemmal membrane Ca pump (I_{SLCaP}) from the Shannon-Bers model (2). We removed the passive leak current (I_{leak}) for this study. The ordinary differential equations are solved by the Euler method. Time step is 0.01 ms. The program codes are written in C++. Equations and parameters are as follows.

Table 1 Constants

Parameter	Description	
R	Gas constant	8.314 $Jmol^{-1}K^{-1}$
T	Absolute temperature	308 K
F	Faraday constant	96.5 C/mmol
$[Ca]_O$	External calcium concentration	1.8 mM
$[Na]_O$	External sodium concentration	136 mM

Intracellular Ca cycling

The intracellular Ca cycling is governed by the following equations.

$$\frac{dc_i^n}{dt} = \beta_i(c_i^n)\left(I_{dsi}\frac{v_s}{v_i} - I_{up} - I_{TCi} + I_{ci}\right),$$

$$\frac{dc_s^n}{dt} = \beta_s(c_s^n)\left(I_{dps}\frac{v_p}{v_s} + I_{NCX} - I_{dsi} - I_{TCs} + I_{cs} - I_{cabk} - I_{slcap}\right),$$

$$\frac{dc_p^n}{dt} = \beta_p(c_p^n)(I_r + I_{Ca} - I_{dps}),$$

$$\frac{dc_{NSR}^n}{dt} = \left(I_{up}\frac{v_i}{v_{NSR}} - I_{tr}\frac{v_{JSR}}{v_{NSR}} + I_{cNSR}\right),$$

$$\frac{dc_{JSR}^n}{dt} = \beta_{JSR}(c_{JSR}^n)\left(I_{tr} - I_r\frac{v_p}{v_{JSR}}\right),$$

where c_i is cytosolic Ca concentration, c_s is the submembrane Ca concentration, c_p is the proximal space Ca concentration, c_{NSR} is the NSR Ca concentration, c_{JSR} is the JSR Ca concentration, v_i is the local cytosolic volume, v_s is the local submembrane space volume, v_p is the local proximal space volume, v_{JSR} is the local JSR volume, β_i is the instantaneous buffer function for c_i, β_s is the instantaneous buffer function for c_s, β_p is the instantaneous buffer function for c_p, β_{JSR} is the instantaneous buffer function for c_{JSR}, I_{dsi} is the diffusive current between c_s and c_i, I_{up} is the SERCA uptake current, I_{ci} is the nearest-neighbor diffusive current for c_i, I_{cs} is the nearest-neighbor diffusive current for c_s, I_{dps} is the diffusive current between c_p

and c_s, I_{NCX} is the sodium-calcium exchange current, I_{CaBk} is the background sarcolemmal membrane Ca flux, I_{SLCaP} is the sarcolemmal membrane Ca pump, I_r is the release current, I_{Ca} is the L-type Ca current, I_{tr} is the JSR refilling current, I_{cNSR} is the nearest-neighbor diffusive current for c_{NSR}, superscript *n* shows the *n*-th compartment.

Diffusive current

The diffusive currents between different compartments are the same as that used by Restrepo et al.

$$I_{dps} = (c_p - c_s)/\tau_p$$
$$I_{tr} = (c_{NSR} - c_{JSR})/\tau_{tr}$$

Table 2 Ca diffusion

Parameter	Description	
τ_i^T	Transverse cytosolic	2.93 ms
τ_i^L	Longitudinal cytosolic	2.32 ms
τ_{NSR}^T	Transverse NSR	7.2 ms
τ_{NSR}^L	Longitudinal NSR	24.0 ms
τ_s^T	Transverse submembrane	1.42 ms
$1/\tau_s^L$	Longitudinal submembrane	0 ms^{-1}
τ_{tr}	JSR refilling time	5.0 ms
τ_{ps}	Proximal to submembrane	0.022 ms
τ_{si}	Submembrane to cytoplasm	0.1 ms

Instantaneous buffer functions

The instantaneous Ca buffer functions are the same as that used by Restrepo et al.

$$\beta_i(c_i) = \left(1 + \sum_b \frac{B_b K_b}{(c_i + Kb)^2}\right)^{-1},$$

$$\beta_s(c_s) = \left(1 + \sum_b \frac{B_b K_b}{(c_s + Kb)^2}\right)^{-1},$$

$$\beta_{JSR}(c_{NSR}) = \left(1 + \frac{K_c B_{CSQN} n(c_{NSR}) + \partial_c(c_{NSR})(cK_c + {c_{NSR}}^2)}{(K_c + c_{NSR})^2}\right)^{-1},$$

where

$$n(c_{JSR}) = \widehat{M} n_M + (1 - \widehat{M}) n_D,$$
$$\widehat{M} = \frac{(1 + 8\rho B_{CSQN})^{1/2} - 1}{4\rho B_{CSQN}},$$
$$\rho(c_{JSR}) = \frac{\rho_\infty c_{JSR}^h}{K^h + c_{JSR}^h}.$$

Troponin C dynamic buffer currents

Troponin C dynamics is the same as that used by Restrepo et al and Shannon et al (1, 2).

$$\frac{d[CaT]_{i,s}}{dt} = I_{TCi,s},$$

where

$$I_{TCi,s} = k_{on}^{T} c_{i,s}\left(B_T - [CaT]_{i,s}\right) - k_{off}^{T}[CaT]_{i,s}.$$

Table 3 Ca buffers

Parameter	Description	
K_{CAM}	Dissociation constant (Calmodulin)	7.0 μM
B_{CAM}	Total concentration (Calmodulin)	24.0 μM
K_{SR}	Dissociation constant (SR sites)	0.6 μM
B_{SR}	Total concentration (SR sites)	47.0 μM
K_{MCa}	Dissociation constant (Myosin(Ca))	0.033 μM
B_{MCa}	Total concentration (Myosin(Ca))	140.0 μM
K_{MMg}	Dissociation constant (Myosin(Mg))	3.64 μM
B_{MMg}	Total concentration (Myosin(Mg))	140.0 μM
K_{SLH}	Dissociation constant	0.3 μM
B_{SLH}	Total concentration	13.4 μM
B_{T}	Total concentration (Troponin)	70.0 μM
$k_{\mathrm{on}}^{\mathrm{T}}$	On rate (Troponin)	0.0327 (μM ms)$^{-1}$
$k_{\mathrm{off}}^{\mathrm{T}}$	Off rate (Troponin)	0.0196 ms^{-1}

SERCA uptake current

The uptake current is the same as that used by Restrepo et al.

$$I_{up} = v_{up}\frac{(c_i/K_i)^H - (c_{NSR}/K_{NSR})^H}{1 + (c_i/K_i)^H + (c_{NSR}/K_{NSR})^H}$$

Table 4 SERCA pump

Parameter	Description	
v_{up}	Strength of uptake	0.0009 μM ms^{-1}
K_{NSR}	K_{m} SR Ca pump reverse mode	1700 μM
K_{i}	K_{m} for SR Ca pump forward mode	0.123 μM
H	Constant	1.787

Sodium-calcium exchange current

The sodium-calcium exchange current is the same as that used by Restrepo et al.

$$I_{NaCa} = \frac{K_a v_{NaCa}\left(e^{\eta z}[Na]_i^3[Ca]_o - e^{(\eta-1)z}[Na]_o^3 c_s\right)}{(t1 + t2 + t3)(1 + k_{sat}e^{(\eta-1)z})},$$

where

$$t1 = K_{mCai}[Na]_o^3\left(1+\left(\frac{[Na]_i}{K_{mNai}}\right)^3\right),$$

$$t2 = K_{mNao}^3 c_s\left(1+\left(\frac{c_s}{K_{mCai}}\right)\right),$$

$$t3 = K_{mCao}[Na]_i^3 + [Na]_i^3[Ca]_o + [Na]_o^3 c_s,$$

$$K_a = \left(1+\left(\frac{K_{da}}{c_s}\right)^3\right)^{-1},$$

$$z = \frac{VF}{RT}.$$

Table 5 Exchanger

Parameter	Description	
v_{NaCa}	Strength of exchanger	1.05 μM/ms
K_{mCai}	Constant	3.59 μM
K_{mCao}	Constant	1.3 mM
K_{mNai}	Constant	12.3 mM
K_{mNao}	Constant	87.5 mM
K_{da}	Constant	0.11 μM
k_{sat}	Saturation factor of the Na-Ca exchanger	0.27
H	Constant	0.35

Release current

The Ca release current is the same as that used by Restrepo et al.

$$I_r = J_{max}\frac{P_o\left(c_{JSR}-c_p\right)}{v_p},$$

where P_O is the fraction of RyR channels that are in the open states. We modified $J_{\max}$ and the RyR gating Markov model described below.

RyR gating Markov model

The RyR channel is modeled as a four-state Markovian model regulated by $[Ca]_{Cleft}$ and $[Ca]_{SR}$. A single CaRU contains 100 RyRs. Each RyR opens independently and stochastically. The volume of the cleft space is 0.00126 μm^3 (disk of radius 0.2 μm and depth 10 nm). Several changes to the Restrepo et al model were made, including:

1) The rates from the closed state to the open state

$$k_{12} = \frac{K_u c_p^2}{K_{cp}^2 + c_p^2}, \qquad k_{43} = \frac{K_b c_p^2}{K_{cp}^2 + c_p^2},$$

where k_{12} is the rate from state 1 (S1) to state 2 (S2), k_{43} is the rate from state 4 (S4) to state 3 (S3), c_p is $[Ca]_{Cleft}$, Ku, K_{cp},Kb are constants.

2) The rates from the open state to the closed state to fit the experimental observation of the mean open times (0.7~1.9 ms) (3)

$$k_{21}=0.5\ \text{ms}^{-1},\quad k_{34}=3.3\ \text{ms}^{-1}$$

The other equations are the same as that used by Restrepo et al.

$$k_{14}=\frac{\widehat{M}(c_p)\tau_b^{-1}B_{CSQN}}{B_{CSQN}^0},$$

$$k_{23}=\frac{\widehat{M}(c_p)\tau_b^{-1}B_{CSQN}}{B_{CSQN}^0},$$

$$k_{41}=\frac{1}{\tau_u},$$

$$k_{32}=\frac{k_{41}k_{12}}{k_{43}}.$$

Table 6 SR Ca release

Parameter	Description	
J_{max}	Strength of Ca release flux	0.2646 μm^3 ms^{-1}
B_{CSQN}	CSQN concentration	400 μM
K_C	Dissociation constant of CSQN	600 μM
n_M	Buffering capacity of CSQN monomers	15
n_D	Buffering capacity of CSQN dimers	35
ρ_∞	Asymptotic ratio of dimers to monomers	5000
K_{NSR}	K_m SR Ca pump reverse mode	1700 μM
H	Constant	1.787
K_u	CSQN-unbound opening rate	5.0 ms^{-1}
K_b	CSQN-bound opening rate	0.005 ms^{-1}
K_{cp}	Constant	100 μM
τ_u	CSQN unbinding timescale	1250 ms
τ_b	CSQN binding timescale	4 ms
h	Dimerization exponent	10
K	Dimerization constant	1400

Background sarcolemmal membrane Ca flux (I_{CaBk})

We added the background sarcolemmal membrane Ca flux (I_{CaBk}) from the Shannon-Bers model (2).

$$I_{CaBk}=\bar{G}_{CaBk}(V-E_{Ca}),$$

where

$$E_{Ca}=\frac{RT}{F}\ln\frac{[Ca]_O}{c_s}$$

Sarcolemmal membrane Ca pump (I_{SLCaP})

We added the sarcolemmal membrane Ca pump (I_{SLCaP}) from the Shannon-Bers model

$$I_{SLCaP} = \frac{Q_{SLCaP} V_{max}}{1 + \left(\frac{K_m}{c_s}\right)^H}$$

Table 7 parameters for I_{CaBk} and I_{SLCaP}

Parameter	Description	
G_{CaBk}	Strength of the background SL Ca flux	0.00084 μM ms^{-1}
V_{max}	Strength of the SL Ca pump	0.0022 μM ms^{-1}
K_m	Constant	0.5 μM
H	Constant	1.6
Q_{SLCaP}	Constant	2.35

REFERENCES

1. Restrepo, J. G., J. N. Weiss, and A. Karma. 2008. Calsequestrin-Mediated Mechanism for Cellular Calcium Transient Alternans. Biophysical Journal 95:3767-3789.
2. Shannon, T. R., F. Wang, J. Puglisi, C. Weber, and D. M. Bers. 2004. A Mathematical Treatment of Integrated Ca Dynamics within the Ventricular Myocyte. Biophysical Journal 87:3351-3371.
3. Györke, I., and S. Györke. 1998. Regulation of the Cardiac Ryanodine Receptor Channel by Luminal Ca2+ Involves Luminal Ca2+ Sensing Sites. Biophysical Journal 75:2801-2810.